

Electrical properties of Yttrium(Y) doped LaTiO_3

Nondon Lal Dey ^{1,*}, Shuvasish Chowdhury ¹, Islam Uddin Shipu ², Muhammad Ihsan Ibn Rahim ¹, Debangshu Deb ³ and Md Rafid Hasan ⁴

¹ Department of Physics, University of Louisiana at Lafayette, 104 E University Ave, Lafayette, LA, 70504, USA

² Department of Chemistry, The University of Texas Rio Grande Valley, 1201 W University Drive, Edinburg, Texas, TX-78539, USA

³ Department of Mathematics, University of Louisiana at Lafayette, 104 E University Ave, Lafayette, LA, 70504, USA

⁴ Department of Physics and Optical science, University of North Carolina at Charlotte, 9201 University City Blvd, Charlotte, NC 28223, USA.

International Journal of Science and Research Archive, 2024, 12(02), 744–767

Publication history: Received on 08 June 2024; revised on 15 July 2024; accepted on 18 July 2024

Article DOI: <https://doi.org/10.30574/ijrsra.2024.12.2.1321>

Abstract

The perovskite structure has shown enormous utility in many facets of science in the past 50 years. From applications in high-temperature superconductors to piezoelectric sensors, the perovskite structure has been used in a wide array of cutting-edge areas of solid-state physics and materials science. LaTiO_3 has a perovskite type crystal structure. It undergoes three phase transitions. At 50-100 K LaTiO_3 undergoes a magnetic phase transition. Jahn–Teller phase transition occurs between 100 K and 300 K. Also, insulator-metal (I-M) transition occurred at 500-550k. On the other hand, YTiO_3 also have perovskite type crystal structure. It undergoes I-M phase transition around 750 K. We are interested to know the effect of the electrical and dielectric properties by replacing La with Y (Yttrium). To investigate the electrical and dielectric properties of $\text{La}_{1-x}\text{Y}_x\text{TiO}_3$ [$x = 0.0, 0.2, 0.3, 0.4$ and 0.6] system, samples have been prepared by solid state reaction method. To confirm the crystal structure, room temperature X-ray diffractions were performed and no extra peak was observed. The measurement of frequency dependence dielectric constant shows that the decreases in dielectric constant observed with increase in frequency and the value of dielectric constant increase with increasing concentration of Y (Yttrium). We also observed that loss tangent decrease with increasing frequency and increase in concentration of Y (Yttrium) results to decrease in the value of loss tangent. The cole-cole plot shows that the grain size decrease with increasing concentration of Y (Yttrium), as a result resistivity decrease while conductivity increases with increasing concentration of Y (Yttrium).

Keywords: Perovskite Structure; High-temperature Superconductor; Piezoelectric sensors; LaTiO_3 ; Magnetic Phase Transition; Dielectric Properties; Grain Size; Conductivity; Yttrium Concentration.

1. Introduction

Perovskites are a large family of isotopic crystalline ceramics. The general chemical formula of perovskite compound is ABX_3 , where A and B are cations of quite different sizes and X is an anion [1]. The highly versatile ABX_3 perovskite crystal structure is composed of three-dimensional networks of corner-sharing BX_6 octahedral, and the A-site cations fill the 12 coordinated cavities formed by the BX_6 network [2]. The substitution of different cations into the A and B position is also possible and these so called complex perovskites may have ordered and disordered variants. We are interested to study the substitutions of Y on the La side in the LaTiO_3 .

* Corresponding author: Nondon Lal Dey

Lanthanum cobalt oxide LaTiO_3 has a rhombohedrally distorted perovskite structure with the crystal space group of $\bar{R}3c$ [1-3] [3]. Raccach and Goodenough have reported that the crystal space group varies with increasing temperature from $\bar{R}3c$ to $\bar{R}3$ around 650K [4]. In the high temperature phase, two kinds of inequivalent Ti atoms order preferentially on alternate (111) Ti [4] They have also reported a first order insulator-to-metal phase transition at 1210K accompanied with an abrupt drop of the rhombohedral angle from 60.4° to 60° keeping $\bar{R}3$ symmetry through the transition [2]. In addition, they reported an endothermic first order transition at 1210 K, and higher order phase transitions at around 550 and 900K from the differential thermal analysis [5]. A powder neutron diffraction study has revealed that LaCoO_3 has $\bar{R}3c$ symmetry between 4.2 and 1248 K, with possible exception at 668K [4]. According to the study, the rhombohedral angle remains 60.3° even at 1248 K. Their study does not support the first order phase transition at 1210K [6].

The urgent important Issue for development of environment is to control automobile and industrial emission of toxic gases by using the catalytic converters. Lanthanum cobaltite (LaTiO_3) is one of the most promising catalytic materials that have many practical applications for its excellent physical and chemical properties [4]. This catalyst can be used for combustion, automobile exhaust and waste gas purification. Moreover, it can be used as an electrode material for solid-state fuel cells, gas sensors [6] and thermoelectric power production for its excellent thermoelectric properties.

Perovskite materials like LaTiO_3 have many technological aspects. Mixed ionically and electrically conducting LaTiO_3 are important electrode materials such as Solid Oxide Fuel Cells (SOFC) and Gas Sensors [5]. Research is also going on their potential use as chemical reactors and gas separation membrane. The most critical characteristic of these types of materials are their electrical conductivities including total conductivity, ionic conductivity and electronic conductivity [7].

LaTiO_3 has much attraction due to the magnetic property which originates from the spin state of Ti^{3+} ions. At low temperature, LaTiO_3 is nonmagnetic, because Ti^{3+} ion being in LS state with six electrons in the t_{2g} levels and empty e_g states (LS, $t_{2g}^6 e_g^0$, $S = 0$). At 50-100 K LaTiO_3 undergoes a magnetic phase transition. This transition originates from the thermal population of excited Ti^{3+} states that are either of intermediate spin (IS, $t_{2g}^5 e_g^1$, $S = 1$) or high spin (HS, $t_{2g}^4 e_g^2$, $S = 2$) character. Keisuke Sato et al. have observed that the magnetization increase with increasing temperature shows a maximum at around 100 K then decreases [8]. A second transition at 500–550 K is of an insulator-metal (I-M) kind and is accompanied by a further change of paramagnetic properties. K. Knizek et al. have observed that the magnetic and electronic transitions are accompanied also by subtle changes in the crystal structure, which is of the Rhombohedral Perovskite type $\bar{R}3c$ [9]. The effects are of two kinds. First, the ionic radius of Co^{3+} increases from $r_{LS} = 0.545 \text{ \AA}$ to $r_{IS} = 0.56 \text{ \AA}$ or $r_{HS} = 0.6 \text{ \AA}$ [10]. Second, Co^{3+} ion in IS or HS state is Jahn-Teller active and corresponding distortion of the TiO_6 Octahedra may arise. In particular, a monoclinic distortion of the LaTiO_3 structure (space group 12/a) and Jahn-Teller distortion of TiO_6 Octahedral was found recently by G. Maris et al in single-crystal X-ray diffraction between 100 and 300 K [11]. The analogous compound YTiO_3 also undergoes a diamagnetic-paramagnetic transition, but more diffusive and shifted to higher temperatures between 450 and 800 K [12]. The I-M transition occurs around 750 K.

We are interested to dope Y on the La side of the compound LaTiO_3 to study the effect of Y on the density, porosity, electrical and dielectrical properties. For these purpose samples $\text{La}_x\text{Y}_{1-x}\text{TiO}_3$ with concentration $x = 0.0, 0.2, 0.3, 0.4$ and 0.6 are prepared. For sample preparation we have used La_2O_3 , Y_2O_3 , and Ti_3O_4 . Yttrium oxide is the most thermodynamically stable compound in the oxide group. It is resistant to many reactive molten metals such as titanium or uranium. In its industrial application as a pure ceramic, Yttrium oxide is still a relatively new material. Particularly due to its extremely high temperature stability up to 745°C and its outstanding resistance to alkaline metals with high oxygen affinity, this material is used in numerous special applications.

To confirm the crystal structure, room temperature X-ray diffractions are performed. The electric and dielectric properties are measured by impedance analyzer and the data is analyzed by origin software. The measurement of frequency dependence dielectric constant shows that the decreases in dielectric constant observed with increase in frequency and the value of dielectric constant increase with increasing concentration of Y (Yttrium). We also observed that loss tangent decrease with increasing frequency and increase in concentration of Y (Yttrium) results to decrease in the value of loss tangent. The cole-cole plot shows that the grain size decrease with increasing concentration of Y (Yttrium), as a result resistivity decrease while conductivity increases with increasing concentration of Y (Yttrium).

Rest of the plan of the research is as follows: in chapter 2 we give a brief description of different type of crystal structure, theory of Bragg law, different measurement of electrical and dielectric properties such as dielectric constant, loss

tangent, resistivity, conductivity, cole-cole plot. In chapter 3 we discussed the detail of the sample preparation technique that have been used in the thesis work. In chapter 4 we give the Calculation of different sample made for the thesis work. In chapter 5 we briefly discuss the result and discussion. Finally, in chapter 6 we summarized our experimental results.

2. Experimental theory

2.1. Crystal Structure

A lattice is a regular periodic array of points in space. A crystal structure is formed only when the group of atoms is arranged identically at the lattice point. The group of atoms or molecules is called a basis. A lattice is merely a mathematical abstraction which is actually an imaginary concept [13]. So, the relation becomes

Lattice + Basis = Crystal structure.

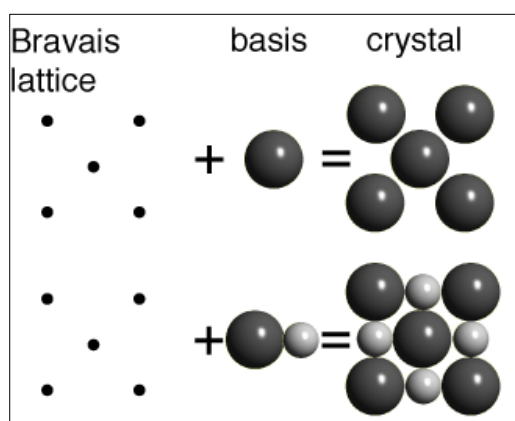


Figure 1 Crystal Structure

2.2 Bravais Lattice

The Bravais lattices are the distinct lattice types which when repeated can fill the whole space. The lattice can therefore be generated by three unit vectors, \mathbf{a}_1 , \mathbf{a}_2 and \mathbf{a}_3 and a set of integers k , l and m so that each lattice point, identified by a vector \mathbf{r} , can be obtained from equation [14]

$$\mathbf{r} = k \mathbf{a}_1 + l \mathbf{a}_2 + m \mathbf{a}_3 \tag{2.1}$$

There are basically two types of Bravais lattice-

- 1) Two dimensional Bravais lattice
- 2) Three dimensional Bravais lattice

2.1.1. Two dimensional /Surface Bravais lattice:

In two dimensions there are 5 distinct Bravais lattice. They are summarized in the below table 1 [15].

Table 1 Two dimensional Bravais lattice

Lattice	Conventional Unit cell	Axes of Conventional Unit cell
Oblique	Parallelogram	$a \neq b, \gamma \neq 90$
Rectangular	Rectangle	$a \neq b, \gamma = 90$
Rectangular centered	Rectangle	$a \neq b, \gamma = 90$
Square	square	$a = b, \gamma \neq 90$
Hexagonal	60° rhombus	$a = b, \gamma = 120$

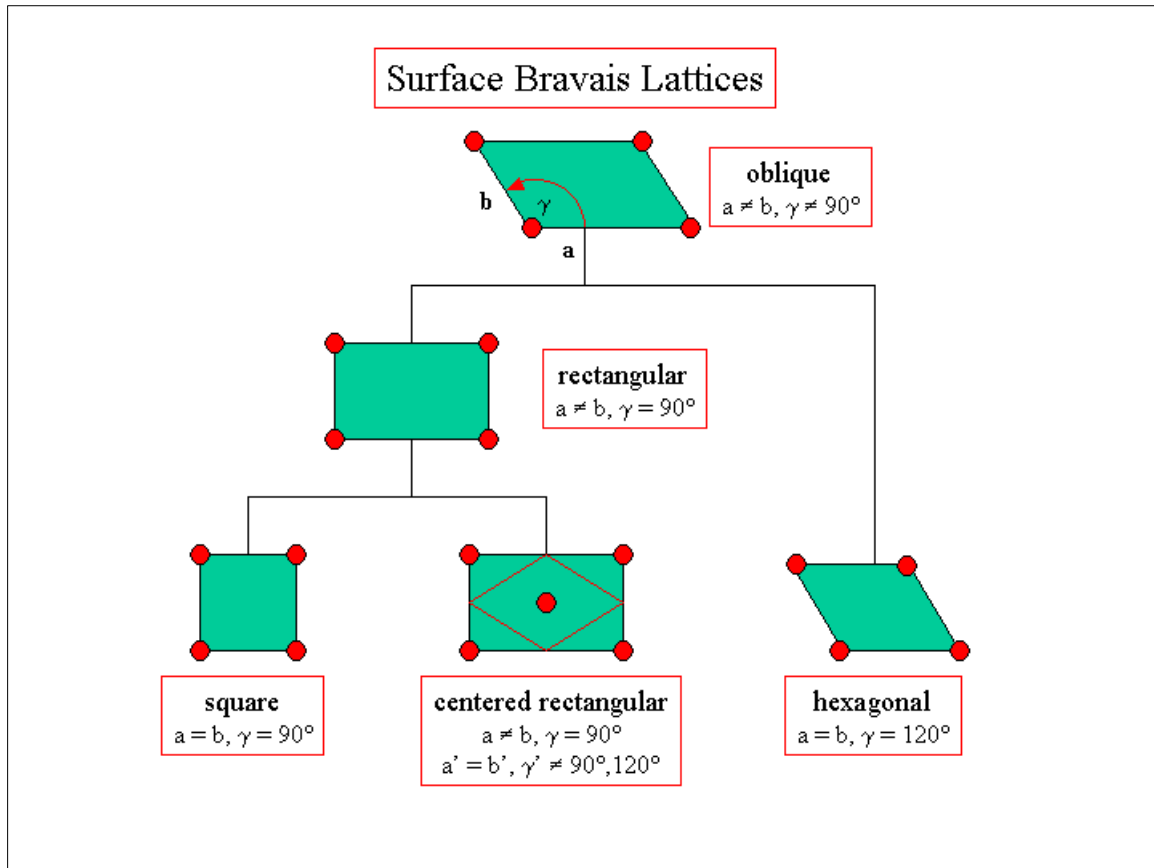


Figure 2 Two dimensional Bravais lattice [16]

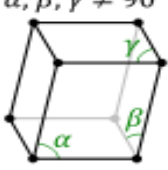
2.1.2. Three dimensional Bravais Lattice

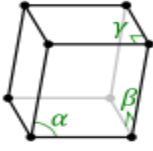
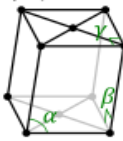
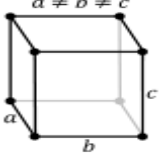
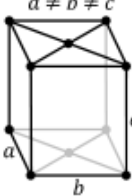
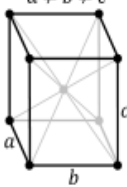
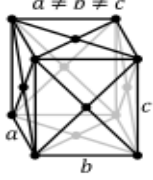
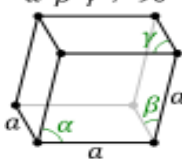
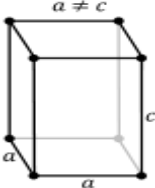
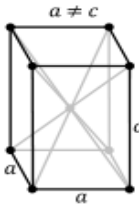
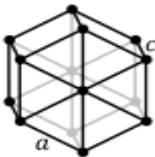
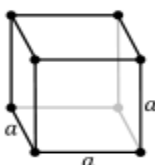
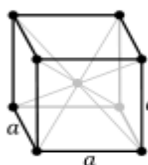
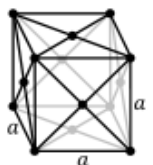
The point symmetry groups in three dimension requires the 14 different lattice types listed in Table 2. These lattice types are arrived at by combining one of the seven lattice systems with one of the lattice centering.

The lattice centering are [17]:

- Primitive centering: Lattice points at the cell corners only.
- Body centered: One additional lattice point at the center of the cell.
- Face centered: One additional lattice point at center of each of the faces of the cell.
- Base centered: One additional lattice point at the center of each of one pair of cell faces.

Table 2 Three dimensional Bravais lattice [18]

Lattice Systems	Characteristic Symmetry elements	Simple	Base-centered	Body-centered	Face centered
Triclinic	None	$\alpha, \beta, \gamma \neq 90^\circ$ 			

Monoclinic	One 2-fold rotation axis	$\alpha \neq 90^\circ$ $\beta, \gamma = 90^\circ$ 	$\alpha \neq 90^\circ$ $\beta, \gamma = 90^\circ$ 		
Orthorhombic	Three mutually perpendicular 2-fold rotation axes	$a \neq b \neq c$ 	$a \neq b \neq c$ 	$a \neq b \neq c$ 	$a \neq b \neq c$ 
Rhombohedral	One 3-fold rotation axis	$\alpha = \beta = \gamma \neq 90^\circ$ 			
Tetragonal	One 4-fold axis and two 2-fold axes normal to the 4-fold axes	$a \neq c$ 		$a \neq c$ 	
Hexagonal	One 6-fold rotation axes				
Cubic	Four 3-fold rotation axis				

The general lattice is triclinic and there are 13 special lattices. These are grouped for convenience into systems classified according to seven types of cell. The division into systems is expressed in the table in terms of axial relations that describe the cells [19].

2.2. X-ray Diffraction

Bragg reflection is a coherent elastic scattering in which the energy of the X-ray is not changed on reflection. If a beam of monochromatic radiation of wavelength λ is incident on a periodic crystal plane at an angle θ and is diffracted at the same angle as shown in Fig. 2.3, the Bragg diffraction condition for x-rays is given by [16]

$$2d \sin\theta = n\lambda \quad (2.2)$$

where d is the distance between crystal planes and n is the positive integer which represents the order of reflection. Equation (2.2) is known as Bragg law. This Bragg law suggests that the diffraction is only possible when $\lambda \leq 2d$ [20]. For this reason we cannot use the visible light to determine the crystal structure of a material. The X-ray diffraction (XRD) provides substantial information on the crystal structure.

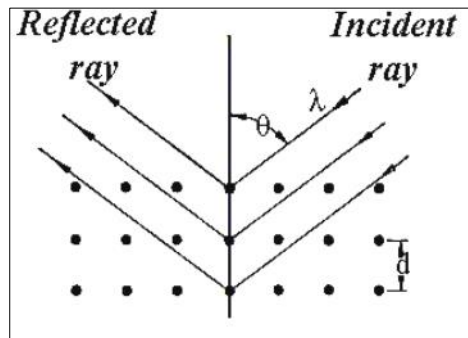


Figure 3 Bragg law of diffraction.

X-ray diffraction was carried out with an X-ray diffractometer for all the samples. For this purpose monochromatic $\text{Cu-K}\alpha$ radiation was used. The lattice parameter for each peak of each sample was calculated by using the formula [15]

$$a = d\sqrt{h^2 + k^2 + l^2} \quad (2.3)$$

where h , k and l are the indices of the crystal planes. To determine the exact lattice parameter for each sample, Nelson-Riley method was used. The Nelson-Riley function $F(\theta)$ is given as

$$F(\theta) = \frac{1}{2} \left[\left(\frac{\cos^2\theta}{\sin\theta} \right) + \left(\frac{\cos^2\theta}{\theta} \right) \right] \quad (2.4)$$

The values of lattice constant 'a' of all the peaks for a sample are plotted against $F(\theta)$. Then using a least square fit method exact lattice parameter 'a₀' is determined. The point where the least square fit straight line cut the y-axis (i.e. at $F(\theta) = 0$) is the actual lattice parameter of the sample. The theoretical density ρ_{th} was calculated using following expression:

$$\rho_{th} = \frac{2M}{N_A a_0^3} \text{ g/cm}^3 \quad (2.5)$$

where N_A is Avogadro's number ($6.02 \times 10^{23} \text{ mol}^{-1}$), M is the molecular weight. The porosity was calculated from the relation $\left\{ 100(\rho_{th} - \rho_B) / \rho_{th} \right\} \%$, where ρ_B is the bulk density [9].

2.3. Bulk Density measurement

The density of the sintered and polished pellet samples was measured using the following method. First, pellet mass was measured via a precision balance (SHIMADZU-AY220) [15]. Then the volume was measured using slide calipers. With these two values, the density of a pellet can be calculated as the following formula:

$$\rho = \frac{\text{mass}}{\text{volume}}$$

2.4. Electrical properties

Ceramics are mostly covalently bonded material hence electrical non-conducting or insulator. Importance of particular property depends on the application demand. For instance, dielectric strength is an important parameter for application of ceramic as insulators used in power transmission line, load bearing general insulators, in house hold appliance, etc [21]. In this kind of applications where frequency does not exceed 1 kHz, the breakdown strength, measured in kV/cm, and mechanical strength are prime important factors. The dielectric constant (ϵ') or loss factor (ϵ'') does not matter much. On the other hand, for capacitor and electronics applications just the opposite is required. The values of ϵ' and ϵ'' are of prime importance, not only their room temperature values but also as function of temperature and frequency. In the following sections basic concept and factors governing dielectric constant, dielectric losses are discussed. Materials are treated as polycrystalline and dielectrics [15].

2.5. Dielectric properties Measurement

For high frequency application, the desirable property of a dielectric is high dielectric constant with low loss. One of the most important goals of dielectric research is to fulfill this requirement. The techniques of dielectric properties measurement and frequency characteristics of the present samples are described in sections 2.6.1.

2.5.1. Techniques for the Permeability Measurement

Measurements of dielectrics properties normally involve the measurements of the change in capacitance and loss of a capacitor in presence of the dielectric materials. The behavior of a capacitance can now be described as follows. We assume an ideal loss less air capacitor of capacitance C_0 . On insertion of a dielectric material with permittivity ϵ , the capacitance will be ϵC_0 . The dielectric (ϵ') and electrical (impedance, z') properties and measurements on disk shaped specimens were carried out at room temperature on all the samples in the frequency range 1 KHz – 10 KHz. The dielectric constant ϵ' were calculated using the following relations [4]: $\epsilon' = C/C_0$ and $\epsilon'' = \epsilon' \tan \delta$, where C is the capacitance of the sample materials and $C_0 = \epsilon_0 A/d$ is derived geometrically [20]. Here C_0 is the capacitance of the capacitor without the dielectric materials, d is the thickness of the capacitor and $A (= \pi r^2)$ is the area of cross section of the disk shape sample.

2.5.2. Dielectric constant

The overall Dielectric constant (ϵ') of an insulator material is given by the relation [22]:

$$D = \epsilon E_0 = \epsilon_0 \epsilon' E_0 \quad (2.6)$$

D represents the electric displacement, E the electric field in the dielectric, ϵ' the dielectric constant and ϵ_0 permittivity of vacuum. The electric displacement describes the extent to which the electric field has been altered by the presence of the dielectric material. The dielectric constant ϵ' is an intrinsic property of a material and a measure of the ability of the material to store electric charge relative to vacuum. It is measured indirectly from the capacitance of a capacitor in which the material is used as electrode separator or dielectric. From Eq. 2.7 and the capacitive cell illustrated in Fig. 2.4, the dielectric constant ϵ' , total charge Q (coulombs) and capacitance C (farads) can be developed as follows [23]:

$$\epsilon' = \frac{D}{\epsilon_0 E} = \frac{Q/A}{\epsilon_0 V/d} \quad (2.7)$$

Therefore,
$$Q = \epsilon_0 \epsilon' \frac{A}{d} V = CV \quad (2.8)$$

Where,
$$C = \epsilon_0 \epsilon' \frac{A}{d} \tag{2.9}$$

$$C_0 = \epsilon_0 \frac{A}{d} \tag{2.10}$$

And
$$\epsilon' = \frac{C}{C_0} = \frac{\epsilon}{\epsilon_0} \tag{2.11}$$

Here, A represents the area of the capacitive cell, d its thickness (or gap between the electrodes), C_0 and C the respective capacitance of the capacitor with air and material, V the voltage across the cell, ϵ the material permittivity (F/m) [19]. Thus, ϵ' represents the ratio of the permittivity or charge storage capacity relative to air or vacuum as dielectric. A real capacitor can be represented with a capacitor and a resistor. It is clear from Eq. 2.10 that for a given size capacitor and applied voltage, the higher the ϵ' the higher the capacitance of the capacitor. This is the only variable left with the material scientist to increase the capacitance per unit volume value of capacitor for modern electronics applications.

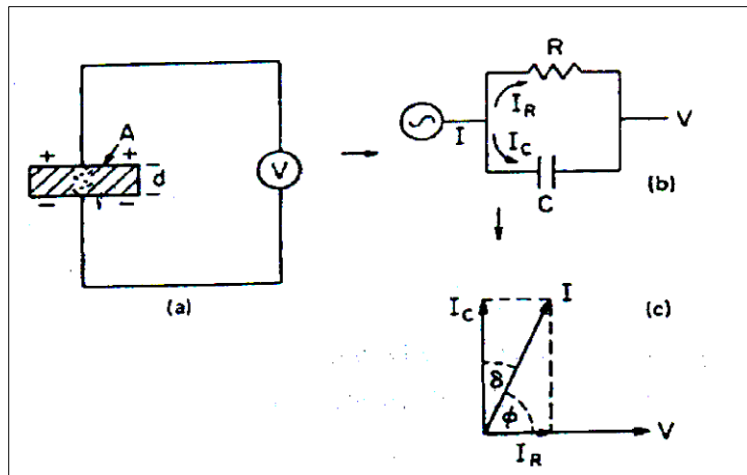


Figure 4 Equivalent circuit diagrams a) Capacitive cell, b) Charging and loss current c) loss tangent [7].

2.6. Dielectric loss

Friction is a macroscopic concept and its explanation in terms of models conceived at a microscopic level has presented difficulties in many branches of physics. Dielectric loss is a special type of friction and the classical and quantum statistical mechanical theories of dielectric loss present the familiar difficulties of principle encountered in a theory of dissipation. Every type of dissipation (dielectric loss) is connected with motions of charge carrier. The effect of their movements in an electric field is called polarization. The total polarization is the sum of various contributions, e.g. electronic polarization due to the relative displacement of electrons and nuclei, dipolar polarization due to orientation of dipoles, and interfacial or Maxwell-Wagner polarization when there are boundaries between the components of a heterogeneous system [17]. The occurrence of dielectric loss can generally be understood as follows: at very low frequencies the polarization easily follows the alternating field, thus its contribution to the dielectric constant is maximal, and no loss occurs. At very high frequencies the field alternates too fast for polarization to arise and there is no contribution to the dielectric constant, and no energy lost in the medium. Somewhere between these two extremes the polarization begins to lag behind the field, and energy is dissipated.

An ideal dielectric would allow no flow of electronic charge, only a displacement of charge via polarization. If a plate of such ideal material were placed between the capacitive cell shown in Fig. 2.4 and a dc voltage was applied, the current through the circuit would decay exponentially to zero with time. But this would not be case if an alternating (sine wave) electric field were applied. In this case Eq. (2.9) may be written as [16]:

$$Q = CVe^{i\omega t} \tag{2.12}$$

Therefore,

$$I = \frac{dQ}{dt} = i\omega CV = i\omega C_0 \epsilon_0 \epsilon' V \tag{2.13}$$

Here, I represent the current flow on discharge of the capacitor in time t. For real dielectric material, the current I has two vector components, real I_R and imaginary I_C

The condition of a lossy (not so good) dielectric illustrated in Fig. 2.4 as an equivalent circuit analogous of a resistance in parallel with the capacitor. The current I_c represents a (watt less) capacitive current proportional to the charge stored in the capacitor. It is frequency dependent and leads the voltage by 90° . On the other hand, the current I_R is ac conduction current in phase with the voltage V, which represents the energy loss or power dissipated in the dielectric. The resultant angle between the current and the voltage is φ somewhat less than 90° . The current in real capacitor lags slightly behind what it would be in an ideal capacitor. The angle of lag is defined as δ and the amount of lag becomes $\tan \delta$ or loss tangent.

Equation (2.10) can be written for real and imaginary part [23],

$$I = I_R + I_C \tag{2.14}$$

$$= \omega C_0 \epsilon_0 \epsilon' V + i\omega C_0 \epsilon_0 \epsilon'' V \tag{2.15}$$

By definition, $\tan \delta = \frac{|I_C|}{|I_R|} = \frac{\epsilon''}{\epsilon'}$ (2.16)

Dielectric loss often attributed to ion migration, ion vibration & deformation and electric polarization. Ion migration is particularly important and strongly affected by temperature and frequency. The losses due to ion migration increase at loss low frequency and the temperature increases.

2.7. The cole-cole plot

Using the Debye model where the dielectric constant is expressed in the following [21]:

$$\epsilon^*(\omega, T) = \epsilon' - i\epsilon'' \tag{2.17}$$

where ϵ^* is the complex dielectric permittivity, ϵ' (energy dissipated per cycle) is the real part of complex dielectric permittivity and ϵ'' (energy stored per cycle) is the imaginary part of the complex dielectric permittivity.

$$\epsilon' = \epsilon_\infty + \frac{\epsilon_0 - \epsilon_\infty}{1 + \omega^2 \tau^2} \tag{2.18}$$

$$\epsilon'' = \frac{(\epsilon_0 - \epsilon_\infty)\omega\tau}{1 + \omega^2 \tau^2} \tag{2.19}$$

where ϵ_0 is the static or relaxed dielectric constant at ($\omega = 0$), ϵ_∞ is the high frequency or unrelaxed dielectric constant and the quantity τ is a characteristic time constant, usually called the dielectric relaxation time, it refers to a gradual change in the polarization following an abrupt change in applied field

The difference in dielectric constant measured at low and high frequencies is called the strength of the relaxation. By eliminating the parameter the $\omega\tau$ between Eqns. (2.18) and (2.19), it can be obtained [16]

$$\left(\epsilon' - \frac{\epsilon_0 - \epsilon_\infty}{2}\right)^2 + \epsilon''^2 = \left(\frac{\epsilon_0 - \epsilon_\infty}{2}\right)^2. \quad (2.20)$$

This is the equation of a circle, center $[(\epsilon_0 + \epsilon_\infty)/2, 0]$, radius $(\epsilon_0 - \epsilon_\infty)/2$, so that a plot of ϵ' against ϵ'' should give a semicircle.

Relaxation in dielectric materials show broader dispersion curves and lower loss maxima than those predicted by the Debye model and $\epsilon' - \epsilon''$ curve falls under the semicircle. This lead Cole and Cole [6] to suggest the following semi-empirical equation for the dielectric relaxation of dielectric materials.

$$\epsilon^* = \epsilon_\infty + \frac{\epsilon_0 - \epsilon_\infty}{1 + (i\omega\tau)^\alpha} \quad (2.21)$$

where $0 < \alpha \leq 1$. The parameter α describes the deviation from the ideal Debye Equation. If ϵ'' is plotted against ϵ' , this equation represents a circle with the center at $((\epsilon_0 + \epsilon_\infty)/2, 0)$ and radius $(\epsilon_0 - \epsilon_\infty)/2$.

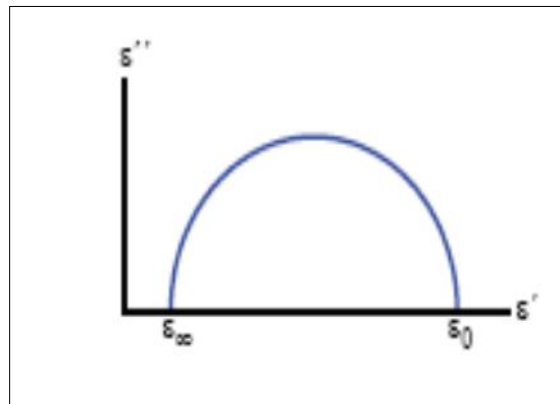


Figure 5 A Cole-Cole circular arc plot constructed from the ϵ', ϵ'' data [1].

3. Sample preparation

3.1. Methods of Sample preparation

Depending on the thermodynamic properties of the compounds to be synthesized, different methods can be used to prepare crystalline solids. There are several well established methods [1], [2], [3] for preparing Perovskite materials. Name of some standardized and well known synthesis methods for Perovskites are given below:

- Solid state reaction method
- Glycine-nitrate route
- Sol - gel method
- Freeze drying
- Spray dryer technique
- chelating precursors (PQ)

For the sample preparation detail process of calcinations, palletization, annealing and Sintering methods are given below:

3.2. Calcinations

Calcinations process is an endothermic decomposition reaction in which an oxy-salt, such as carbonates or hydroxides, decomposes into a solid product (oxide) and releasing the gaseous products. During this decomposition reaction the particle size, its distribution, extent of agglomeration, porosity and morphology are usually established. Calcinations cause the precursors to interact by inter-diffusion of their ions. Calcinations is often the final step in the production of high-purity ceramic powders. During calcinations surface absorbs water vapors, any volatile impurities and carbon dioxide from carbonates are removed and 754 hermos-chemical reaction among the constituent oxides takes place to form the desired compounds. To achieve homogeneous single phase compound double calcinations step is often adopted. The calcinations reaction usually takes place at or above the thermal decomposition or transition temperature. The temperature is usually defined as the temperature at which the standard Gibb's free energy for a particular calcinations reaction is zero [4]. The calcined powders are crashed into fine powders. The ideal characteristics of fine powder are given below:

- Small particle size.
- Narrow distribution in particle size.
- Dispersed particle
- High purity
- Homogenous composition

A small particle size of the reactant powders provides a high contact surface area for initiation of the solid state reaction, diffusion paths are shortened leading to a more efficient completion of reaction. Porosity is easily eliminated if the initial pores are very small. Grain growth during sintering can be better controlled if the initial size is small and uniform.

3.3. Grinding and pelletization

Grinding can be accomplished by any suitable means (e.g., agate mortar and pestle, ball milling etc.). In our present work with $\text{La}_{1-x}\text{Y}_x\text{TiO}_3$ agate mortar and pestle were used for grinding. It helps to mix the constituent materials for sample preparation and also homogenize the compositional variation, which may arise during calcination. If the grinding is coarser the ceramics can have large inter-granular voids and low density. If grinding is too fine, the colloidal properties may interfere with subsequent forming operations. The calcined powders are again ground to very fine powder and mixed with polyvinyl alcohol (PVA) It is used as a binder to reduce brittleness of the pellets, and then pressed (using a hydraulic press) into desired shapes. The binder is used for better compactness among the granules of the materials. For the conventional method of cold pressing, the mixture of finely ground calcined powder with PVA is pressed using a dye-punch by a hydraulic press. The samples are usually circular, rectangular or cylindrical in shape as desired.

3.4. Annealing

Annealing is heat treatment process that alters the physical and sometimes the chemical properties of a material to increase the ductility and reduce its hardness. In our present work annealing was done at 900°C with air flow. In annealing atoms migrate in the crystal lattice and the number of dislocation decrease leading to the change in ductility and hardness [5].

3.5. Sintering

It is often difficult to obtain dense, pore-free ceramic element. Sintering is a process in which fine grains or powders are converted to dense products after heating to an appropriate temperature (below the melting point of the materials). After sintering the intermolecular voids vanish and due to shrinkage of the whole system. Initially a decrease in the volume fraction of pores takes place due to the process of crystalline growth and rearrangement of grains in the powder. At the next stage, pores are completely eliminated by the approach of grain centers and increase of the area of contact between the grains, due to mass transport from the inter-grain contacts towards the pores. The binder present in the sample is burnt out during the sintering process.

There are four categories of sintering present which are dependent on composition and the extent to which second phases are formed during heat treatment. These are:

- Solid state sintering
- Liquid phase sintering
- Vitrification
- Viscous sintering

In our present work solid state sintering was used.

3.5.1. Solid State Sintering

The shaped green body is heated to a temperature that is typically 0.5 – 0.9 of the melting point. No liquid is present and the atomic and atomic diffusion in the solid state produces joining of particle and reduction of porosity. The driving force for sintering is the reduction of surface free energy of the powder. Part of this energy is transferred into interfacial energy grain boundaries in the resulting polycrystalline body [6].

3.5.2. Purpose of Sintering:

The purposes of the sintering process are:

- To bind the particle together so as to impart sufficient strength to the product.
- To make the material more dense by eliminating the pores.
- To homogenize the material by completing the reaction left unfinished in the calcining step.

3.5.3. Steps of Sintering

It is convenient to divide the process into three idealized stages defined in terms of the microstructure, to force correspondence between samples, established sintering model.

The stages are:

- 1st stage: At this stage two things happen to the powder particle when the mobility of surface atoms has become high enough; initially rough surface of particle is smoothed and neck formation occurs.
- 2nd stage: Densification and pore shrinkage occurs. If grain boundaries are formed after the 1st stage, these are new source of atoms for filling up the concave areas which diminishes the outer surface of the particle.
- 3rd stage: Grain growth takes place and the pores break up and form closed spherical bubbles.

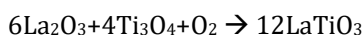
In our present work with $\text{La}_{1-x}\text{Y}_x\text{TiO}_3$, we have used solid state reaction method.

3.6. Description of solid state reaction method

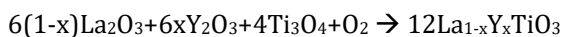
3.6.1. Pre-sintering

Pre-sintering or calcination is defined as the process of obtaining a homogeneous and phase pure composition of mixed power by heating them for certain time at a high temperature. For our sample we take stoichiometric amount of La_2O_3 , Y_2O_3 , TiO_3 . Mixed them under acetone for 3 hours. Then calcined at 800°C for 5 hours with ramp temperature 5°C/min. we mixed the entire sample according to sample calculation from 9 am to 8pm on 08/07/19. Begain the calcination process at 9 pm. It took 3 hours to reach 800°C stays at 800°C for 5 hours and cooled down to room temperature in 3 hours. At 8 am (09/07/19) calcination was ended.

For $x = 0.0$ the following reaction occurred-



For $x = 0.2$ and so on, the following reactions occurred



3.6.2. Pelletization

It is a process of pressing the powder in uni-axial hydraulic press at room temperature by applying a force on it to accelerate the reaction rate. On 09/07/19, we mashed all 8 of our samples for 3hour and measured 0.8gm of each sample. On 10/07/19 we pressed them at 20kN to make palletize sample. We made 2 pallets for each sample.

3.6.3. Sintering

Sintering is defined as the process of obtaining a dense tough body by heating a compacted powder for a certain time at a temperature high enough to significantly promote diffusion, but clearly lower than the melting point. On 10/07/19 at 2 pm we started sintering process.

Sintering temperature was 1300°C. The ramp temperature was 5°C/min. On 11/07/19 at approximately 4.30 am sintering was ended.

3.7. Block diagram for sample preparation

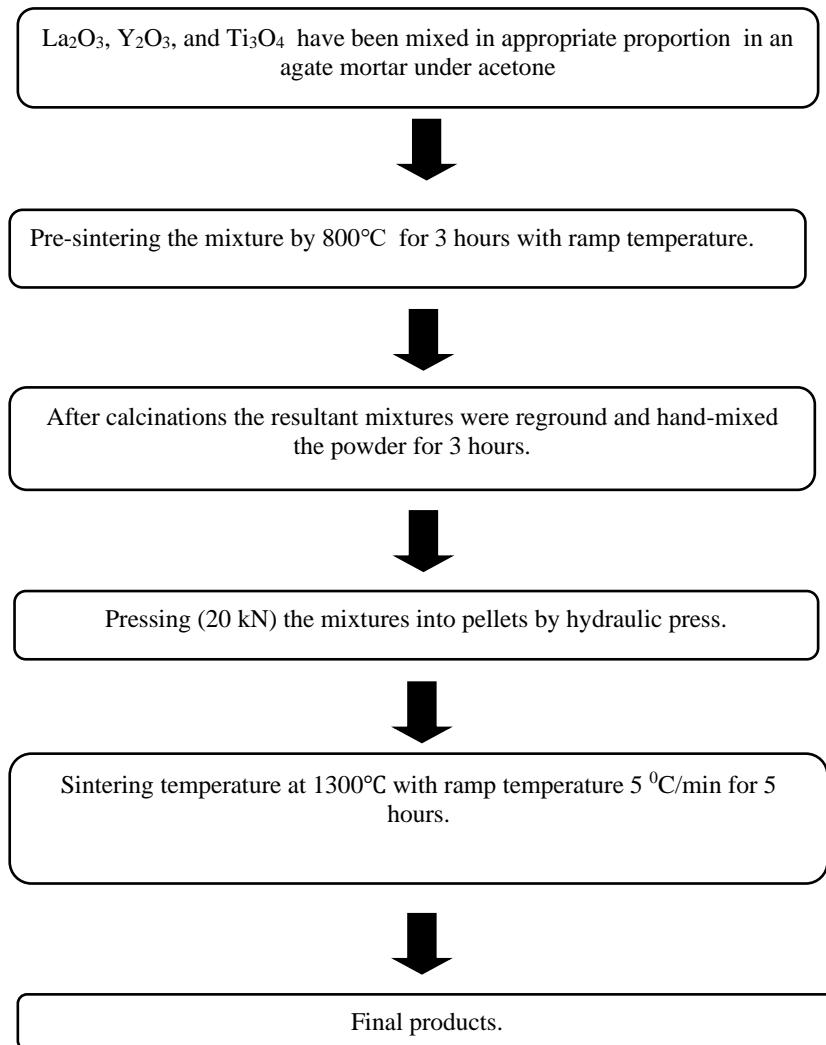


Figure 6 Agate mortar for sample preparation



Figure 7 Hydraulic press



Figure 8 High temperature programmable furnace

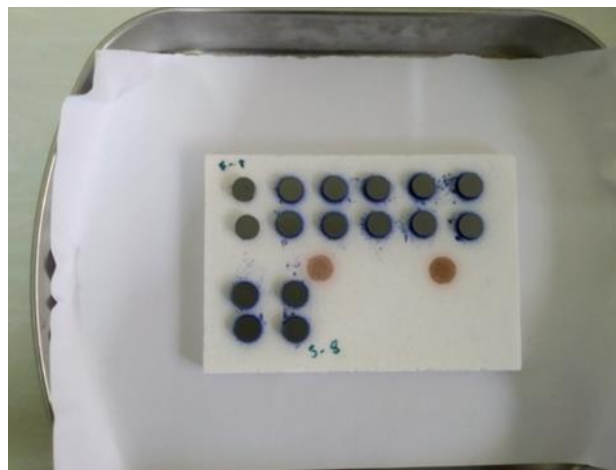


Figure 9 Pallets pro



Figure 10 Impedence analyzer

3.8. Calculation for sample preparation

The symbol of our sample is, $\text{La}_{1-x}\text{Y}_x\text{TiO}_3$ where $x = 0.0, 0.2, 0.3, 0.4$ and 0.6 .

We are going to prepare this polycrystalline bulk sample by using standard solid state reaction technique. The raw compounds are La_2O_3 (99.99%), Y_2O_3 (99.998%) and Ti_3O_4 (99.99%).

The atomic mass of Lanthanum is = 138.905 g

The atomic mass of Yttrium is = 88.905 g

The atomic mass of Titanium is = 58.933 g

The atomic mass of Oxygen is = 16 g

$$\begin{aligned} \text{Atomic mass of } \text{La}_2\text{O}_3 &= (2 \times 138.905) + (3 \times 16) \\ &= 325.807 \text{ g} \end{aligned}$$

$$\begin{aligned} \text{Atomic mass of } \text{Y}_2\text{O}_3 &= (2 \times 88.905) + (3 \times 16) \\ &= 225.807 \text{ g} \end{aligned}$$

$$\begin{aligned} \text{Atomic mass of } \text{Ti}_3\text{O}_4 &= (3 \times 58.933) + (4 \times 16) \\ &= 240.795 \text{ g} \end{aligned}$$

Atomic mass of $\text{La}_{1-x}\text{Y}_x\text{TiO}_3$

$$M_t = (1-x) \cdot M_{\text{La}} + x \cdot M_{\text{Y}} + (M_{\text{Ti}} + M_{\text{O}} \cdot 3)$$

$$= (1-x)*138.905+88.905*x+(58.933+16*3)$$

$$=245.838 - 50x$$

3.8.1. Calculation for 5g $La_{1-x}Y_xTiO_3$ (when $x = 0$)

In this reaction the value of x is 0

$$M_t = 245.838 - 50*0$$

$$= 245.838 - 0$$

$$= 245.838 \text{ g}$$

Atomic mass of La_2O_3 which have to be used in this reaction is

$$M_{La_2O_3} = \frac{(325.807 \times 5)}{(245.835 \times 2)}$$

$$= 3.3132 \text{ g}$$

Atomic mass of Ti_3O_4 which have to be used in this reaction is

$$M_{Ti_3O_4} = \frac{(240.795 \times 5)}{(245.835 \times 3)}$$

$$= 1.63249 \text{ g}$$

Atomic mass of Y_2O_3 which have to be used in this reaction is

$$M_{Y_2O_3} = 0 \text{ g}$$

3.8.2. Calculation for 5g $La_{1-x}Y_xTiO_3$ (when $x = 0.2$)

Now, for $x = 0.2$, the total mass of the compound is

$$M_t = 245.835 - 50*0.2$$

$$= 235.835 \text{ g}$$

Atomic mass of La_2O_3 which have to be used in this reaction is

$$M_{La_2O_3} = \frac{(325.807 \times 0.8 \times 5)}{(235.835 \times 2)}$$

$$= 2.7630 \text{ g}$$

Atomic mass of Y_2O_3 which have to be used in this reaction is

$$M_{Y_2O_3} = \frac{(225.807 \times 0.2 \times 5)}{(235.835 \times 2)}$$

$$= 0.4787 \text{ g}$$

Atomic mass of Ti_3O_4 which have to be used in this reaction is

$$M_{Ti_3O_4} = \frac{(240.795 \times 5)}{(235.835 \times 3)}$$

$$= 1.7017 \text{ g}$$

3.8.3. Calculation for 5g $La_{1-x}Y_xTiO_3$ (when $x = 0.3$)

Now, for $x = 0.3$, the total mass of the compound is

$$M_t = 245.835 - 50 \cdot 0.$$

$$= 230.835$$

Atomic mass of La_2O_3 which have to be used in this reaction is

$$M_{La_2O_3} = \frac{(325.807 \times 0.7 \times 5)}{(230.835 \times 2)}$$

$$= 2.4699 \text{ g}$$

Atomic mass of Y_2O_3 which have to be used in this reaction is

$$M_{Y_2O_3} = \frac{(225.807 \times 0.3 \times 5)}{(230.835 \times 2)}$$

$$= 0.7336 \text{ g}$$

Atomic mass of Ti_3O_4 which have to be used in this reaction is

$$M_{Ti_3O_4} = \frac{(240.795 \times 5)}{(230.835 \times 3)}$$

$$= 1.7385 \text{ g}$$

3.8.4. Calculation for 5g $La_{1-x}Y_xTiO_3$ (when $x = 0.4$)

Now, for $x = 0.4$, the total mass of the compound is

$$M_t = 245.835 - 50 \cdot 0.4$$

$$= 225.835 \text{ g}$$

Atomic mass of La_2O_3 which have to be used in this reaction is

$$M_{La_2O_3} = \frac{(325.807 \times 0.6 \times 5)}{(225.835 \times 2)}$$

$$= 2.1640 \text{ g}$$

Atomic mass of Y_2O_3 which have to be used in this reaction is

$$M_{Y_2O_3} = \frac{(225.807 \times 0.4 \times 5)}{(225.835 \times 2)}$$

$$= 0.9998 \text{ g}$$

Atomic mass of Co_3O_4 which have to be used in this reaction is

$$M_{Ti_3O_4} = \frac{(240.795 \times 5)}{(225.835 \times 3)}$$

$$= 1.7771 \text{ g}$$

3.8.5. Calculation for 5g $La_{1-x}Y_xTiO_3$ (when $x = 0.6$)

Now, for $x = 0.6$, the total mass of the compound is

$$M_t = 245.835 - 50 \times 0.6$$

$$= 215.835$$

Atomic mass of La_2O_3 which have to be used in this reaction is

$$M_{La_2O_3} = \frac{(325.807 \times 0.4 \times 5)}{(215.835 \times 2)}$$

$$= 1.5095 \text{ g}$$

Atomic mass of Y_2O_3 which have to be used in this reaction is

$$M_{Y_2O_3} = \frac{(225.807 \times 0.6 \times 5)}{(215.835 \times 2)}$$

$$= 1.5693 \text{ g}$$

Atomic mass of Co_3O_4 which have to be used in this reaction is

$$M_{Ti_3O_4} = \frac{(240.795 \times 5)}{(215.835 \times 3)}$$

$$= 1.8594 \text{ g}$$

The measurements of different samples were done by Digital Electronic Balance.

Table 3 Calculation for all samples of $La_{1-x}Y_xTiO_3$

Concentration of Y in $La_{1-x}Y_xTiO_3$	Mass of La_2O_3	Mass of Y_2O_3	Mass of Ti_3O_4
0.0	3.3133	0	1.6325
0.2	2.7630	0.4787	1.7017
0.3	2.4699	0.7336	1.7385
0.4	2.1640	0.9998	1.7771
0.6	1.5095	1.5693	1.8594

4. Result and discussion

4.1. Lanthanum yttrium titanium oxide ($La_{1-x}Y_xTiO_3$)

We have prepared the polycrystalline crystal $La_{1-x}Y_xTiO_3$ for the concentration of $x = 0.0, 0.2, 0.3, 0.4$ and 0.6 . To confirm the crystal structure room temperature x-ray diffraction were performed for $x = 0.0, 0.3$ and 0.4 . We have calculated the lattice parameter from the long spectrum to calculate the density and porosity of these samples. On the other hand, we have calculated frequency dependent dielectric constant and loss tangent for the samples with the concentration $x = 0.0, 0.2, 0.4$ and 0.6 at the frequency 10 kHz the conductivity of those samples are calculated which are supported by the cole-cole plot.

5.1.1 Density and porosity of the $La_{1-x}Y_xTiO_3$ Samples

The X-ray diffraction (XRD) patterns for the $La_{1-x}Y_xTiO_3$ samples ($x = 0.0, 0.3, 0.4$) at room temperature are shown in Fig. 5.1, 5.2, 5.3. respectively. We compare our experimental result with [1], and observed that our experimental results are completely identical with them.

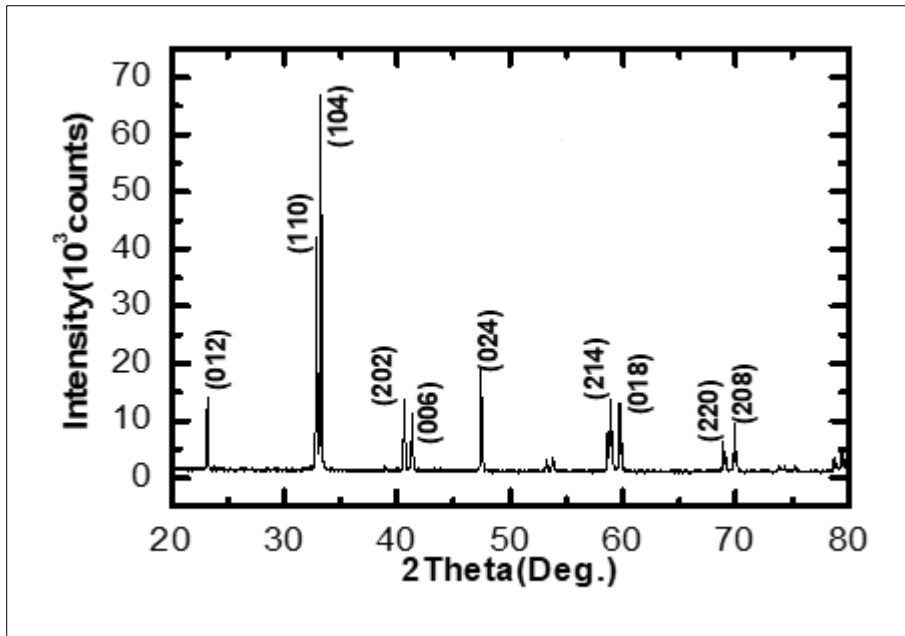


Figure 11 X-ray diffraction pattern of LaTiO₃

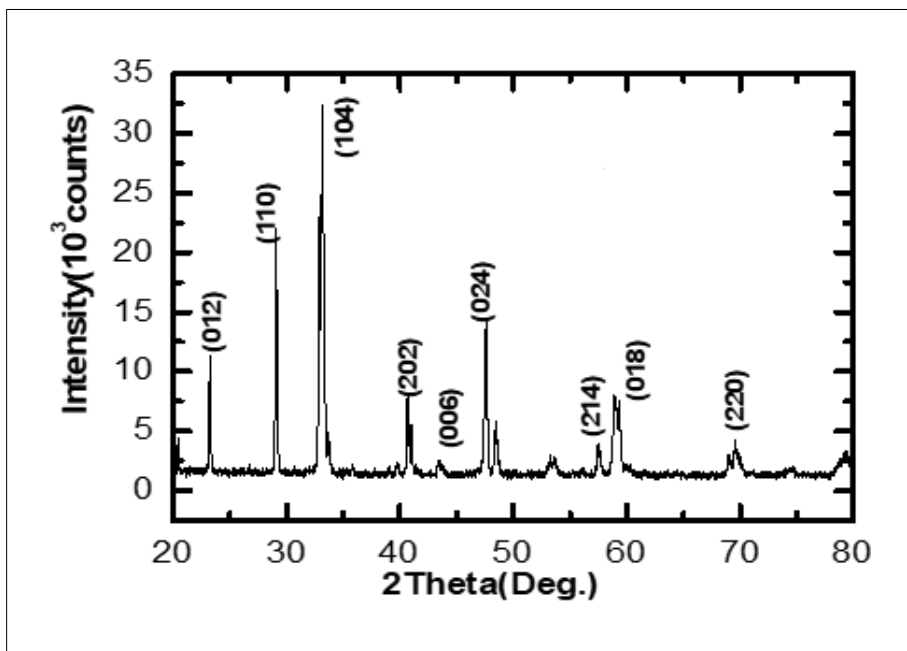


Figure 12 X-ray diffraction pattern of $\text{La}_{0.7}\text{Y}_{0.3}\text{TiO}_3$

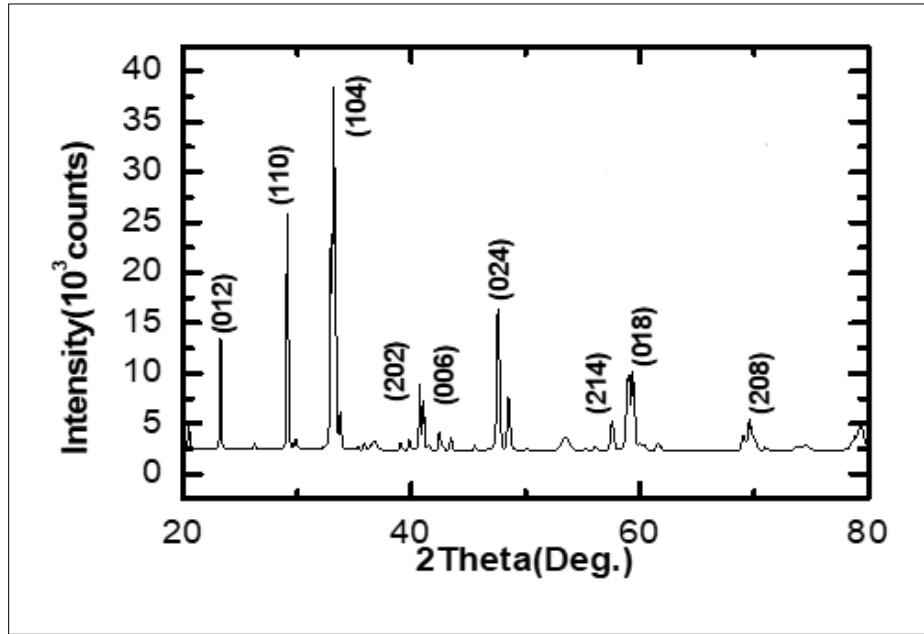


Figure 13 X-ray diffraction pattern of $\text{La}_{0.6}\text{Y}_{0.4}\text{TiO}_3$

From the X-ray diffraction pattern $\text{La}_{1-x}\text{Y}_x\text{TiO}_3$ (with $x = 0.0, 0.3, 0.4$), the positions of the peaks and their corresponding Miller indices are listed in Table-5.1. The bulk densities of samples were calculated by the equation $\left[\rho = \frac{\text{mass}}{\text{volume}}\right]$ and by using the equation $\rho_{th} = \frac{2M}{N_A a_o^3} g/cm^3$ the theoretical density of $\text{La}_{1-x}\text{Y}_x\text{TiO}_3$ are computed. The calculated average densities of the samples are 75% of the theoretical densities. The calculated lattice parameter, density and porosity for the samples are listed in Table-5.

Table 4 X-ray peak positions for $\text{La}_{1-x}\text{Y}_x\text{TiO}_3$ samples

Concentration x in $\text{La}_{1-x}\text{Y}_x\text{TiO}_3$	X-ray peak positions with Miller indices 2θ(degree)							
	(012)	(110)	(104)	(202)	(006)	(024)	(214)	(018)
0.0	23.21	32.79	33.11	40.56	41.42	47.49	58.91	59.86
0.3	23.31	29.07	33.11	40.68	43.44	47.61	57.51	59.36
0.4	23.31	29.17	33.22	40.68	41.20	47.61	57.62	59.43

Table 5 The lattice constant, density, porosity of $\text{La}_{1-x}\text{Y}_x\text{TiO}_3$ samples

Sample composition	Concentration x in $\text{La}_{1-x}\text{Y}_x\text{TiO}_3$	Lattice constant, a_o (Å)	Theoretical density, $\rho_{th}(gm/cm^3)$	Bulk density $\rho_B(gm/cm^3)$	Porosity, P%
$\text{La}_{1-x}\text{Y}_x\text{TiO}_3$	0.0	5.4460	6.14	5.06	21.3331
	0.3	5.4523	6.04	4.73	27.6225
	0.4	5.3340	6.30	4.94	27.417

4.2. Dielectric properties versus frequency of $\text{La}_{1-x}\text{Y}_x\text{TiO}_3$

The frequency dependence of the dielectric constant (ϵ') and tangent loss ($\tan \delta$) at room temperature for the $\text{La}_{1-x}\text{Y}_x\text{TiO}_3$ samples (where $x = 0.0, 0.2, 0.4$ and 0.6) are shown in Fig. 14 & Fig. 15 .

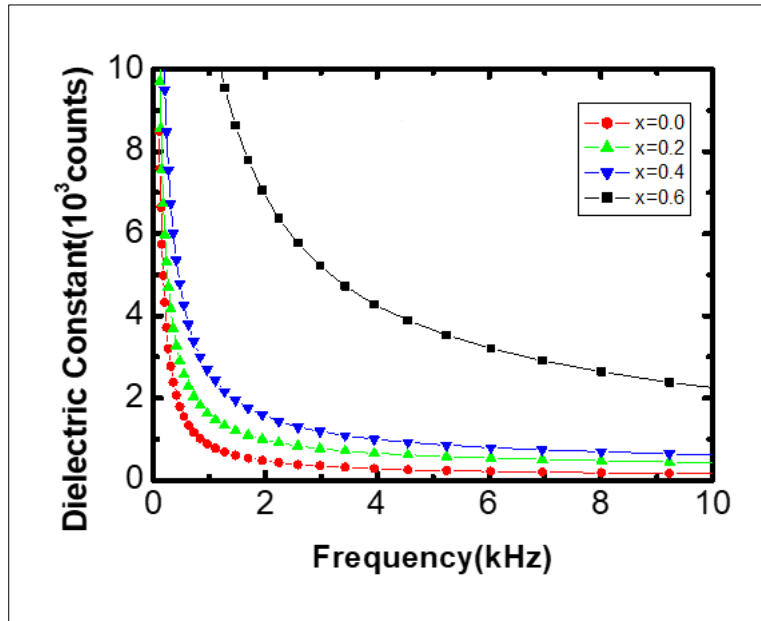


Figure 14 Frequency dependence of the dielectric constant for different samples of $\text{La}_{1-x}\text{Y}_x\text{TiO}_3$

The Fig. 14 shows that dielectric constant decreases with increasing frequency. But with the increase in concentration of yttrium the curve become less steep. Also the Fig. shows that the value of dielectric constant increase with increasing concentration of yttrium.

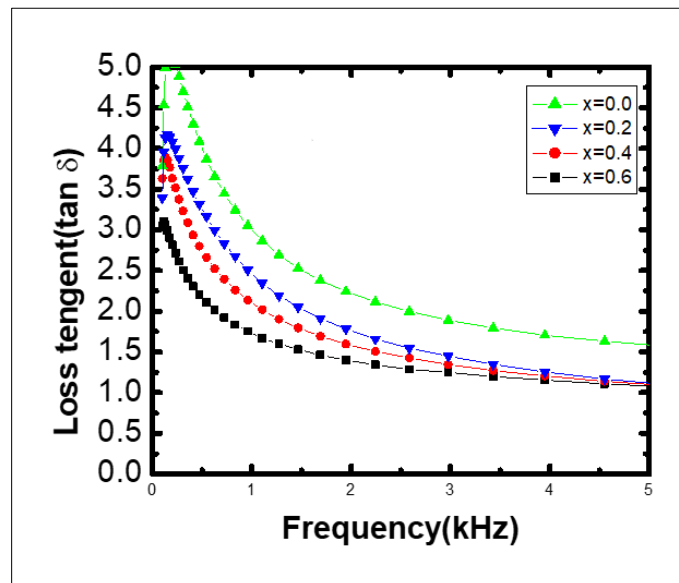


Figure 15 Frequency dependence of the loss tangent for different samples of $\text{La}_{1-x}\text{Y}_x\text{TiO}_3$

Fig. 15 shows that the loss tangent decrease with increasing frequency. Increase in yttrium results to decrease in the value of loss tangent. For high frequency application, the desirable property of a dielectric is high dielectric

constant with low loss. From Fig. 14 & Fig. 15 it is obvious that by increasing concentration of yttrium we can have good dielectric material for high frequency application.

4.3. Electrical properties of $\text{La}_{1-x}\text{Y}_x\text{TiO}_3$

4.3.1. Resistivity and conductivity

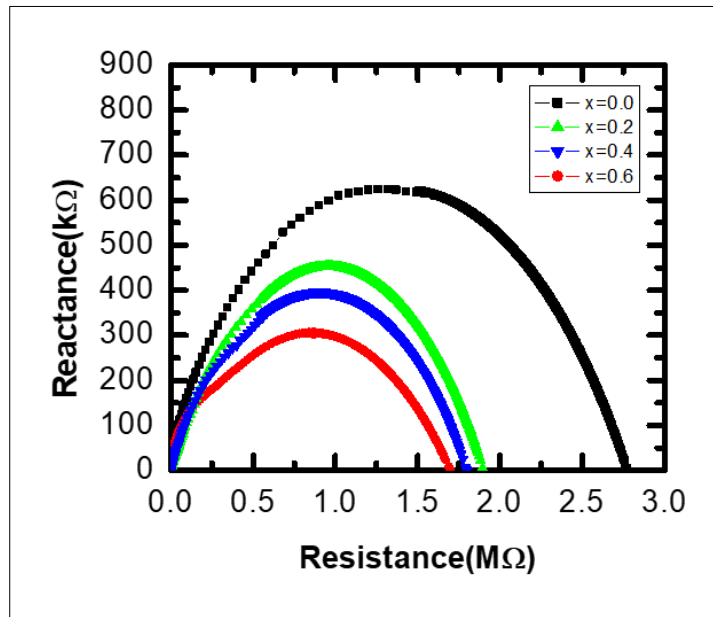


Figure 16 Cole-cole plot with interpolation for different samples of $\text{La}_{1-x}\text{Y}_x\text{TiO}_3$

Fig. 16 shows cole-cole plot for the samples of $\text{La}_{1-x}\text{Y}_x\text{TiO}_3$ with $x = 0.0, 0.2, 0.4$ and 0.6 . It shows that the grain size decreases with increment of yttrium doping. As a result, conductivity increases with increasing concentration of yttrium and resistivity decreases. The curves can be fitted with the Cole-Cole law perfectly, and the fitting parameters are listed in the Table 6.

Table 6 Fitting results of Cole-Cole plot for $\text{La}_{1-x}\text{Y}_x\text{TiO}_3$ samples

$\text{La}_{1-x}\text{Y}_x\text{TiO}_3$				Reading at 10 kHz	
Concentration x in $\text{La}_{1-x}\text{Y}_x\text{TiO}_3$	α	R_{sc} (Ω)	R_{ins} (Ω)	CONDUCTIVITY in (S/m)	RESISTIVITY in (Ω m)
0	0.96	95500	220000	1.15E-04	8.7E+03
0.2	0.54	5950	2775000	1.22E-04	8.20E+03
0.4	0.57	13200	1900000	1.83E-04	5.45E+03
0.6	0.53	8760	1800000	2.78E-04	3.60E+03

In Table-6, the parameter, α describes the deviation from the ideal Debye Equation. The resistance of the semiconducting grain (R_{sc}) and the resistance of the insulating barriers (R_{ins}) values can be obtained by an impedance spectrum analysis [2]. In the Fig. 5.6, according to the article of *Sinclair et al* [3] the non-zero intercept on the resistance-axis gives the resistance of the semiconducting gain (R_{sc}). Since the experimental impedance data at room temperature only cover a part of the arcs for the limit of the measure frequency range, the resistance of the insulating barriers (R_{ins}) was then determined by a data fitting and extrapolation using the well-known Cole-Cole empirical relation.

4.3.2. Capacitance

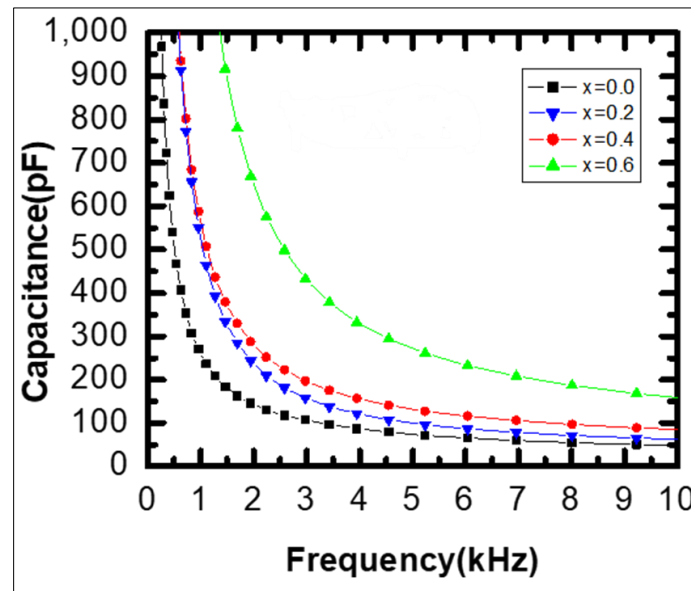


Figure 17 Frequency dependence of the capacitance for the samples of $\text{La}_{1-x}\text{Y}_x\text{TiO}_3$

Fig. 17 shows frequency dependence of the capacitance for the samples $\text{La}_{1-x}\text{Y}_x\text{TiO}_3$ with $x = 0.0, 0.2, 0.4$ and 0.6 . The result shows that the numerical values of the capacitance increases as increasing the doping concentration of Y (Yttrium). But the frequency dependence characteristic appears to have the same property.

5. Conclusion

To investigate the properties of $\text{La}_{1-x}\text{Y}_x\text{TiO}_3$ [$x = 0.0, 0.2, 0.3, 0.4$ and 0.6] system, samples have been prepared by solid state reaction method. To confirm the crystal structure, room temperature X-ray diffractions were performed, and no extra peak was observed. The measurement of frequency dependence dielectric constant shows that the decreases in dielectric constant observed with increase in frequency and the value of dielectric constant increase with increasing concentration of Y (Yttrium). We also observed that loss tangent decrease with increasing frequency and increase in concentration of Y (Yttrium) results to decrease in the value of loss tangent. The cole-cole plot shows that the grain size decrease with increasing concentration of Y (Yttrium), as a result resistivity decrease while conductivity increases with increasing concentration of Y (Yttrium).

Compliance with ethical standards

Disclosure of conflict of interest

There is no conflict of interest.

References

- [1] R. R. Heikes, R. C. Miller, and R. Mazelsky, "Magnetic and electrical anomalies in LaCoO_3 ," *Physica*, vol. 30, no. 8, pp. 1600–1608, 1964, doi: 10.1016/0031-8914(64)90182-X.
- [2] D. O. R. I. O. D. E. Janeiro *et al.*, "No 主観的健康感を中心とした在宅高齢者における健康関連指標に関する共分散構造分析 Title," *Angew. Chemie Int. Ed.* 6(11), 951–952., vol. 3, no. 4, pp. 63–63, 1967, [Online]. Available: http://visitjeju.or.kr/web/bbs/bbsList.do;jsessionid=ZqLJe3DqY4GxEiIBvXK80xgVbeqRXrOIVzfgmdK3hMuvPa9gVklXamfrBo7wzx5l.DB_servlet_engine6?bbsId=TOURSTAT%0Ahttp://search.ebscohost.com/login.aspx?direct=true&AuthType=ip.shib&db=bth&AN=92948285&site=eds-live&
- [3] V. Tuyikeze, L. H. Omari, and F. Fraija, "Investigation of structural, optical and dispersion parameters of $\text{La}_{2-x}\text{ATi}_2\text{O}_7$ (A = Bi, Ce, and Y, with $x = 0.0$ and 0.1) compounds," *Optik (Stuttg.)*, vol. 241, no. February, p. 166953, 2021, doi: 10.1016/j.ijleo.2021.166953.

- [4] V. G. Prabitha *et al.*, “Effect of Yttrium doping on antibacterial and antioxidant property of LaTiO₃,” *Discov. Nano*, vol. 18, no. 1, 2023, doi: 10.1186/s11671-023-03942-1.
- [5] L. He, J. B. Neaton, M. H. Cohen, D. Vanderbilt, and C. C. Homes, “First-principles study of the structure and lattice dielectric response of CaCu₃Ti₄O₁₂,” *Phys. Rev. B - Condens. Matter Mater. Phys.*, vol. 65, no. 21, pp. 2141121–21411211, 2002, doi: 10.1103/PhysRevB.65.214112.
- [6] M. Bradha, S. Hussain, S. Chakravarty, G. Amarendra, and A. Ashok, “Synthesis, structure and total conductivity of A-site doped LaTiO_{3-δ} perovskites,” *J. Alloys Compd.*, vol. 626, pp. 245–251, 2015, doi: 10.1016/j.jallcom.2014.12.033.
- [7] C. Kittel, “Intro to solid state physics by Kittel.pdf.” 1996.
- [8] A. Eciija, K. Vidal, A. Larraaga, L. Ortega-San-Martn, and M. Isabel, “Synthetic Methods for Perovskite Materials; Structure and Morphology,” *Adv. Cryst. Process.*, 2012, doi: 10.5772/36540.
- [9] K. Sato, A. Matsuo, K. Kindo, Y. Kobayashi, and K. Asai, “Field induced spin-state transition in LaCoO₃,” *J. Phys. Soc. Japan*, vol. 78, no. 9, pp. 5–8, 2009, doi: 10.1143/JPSJ.78.093702.
- [10] A. J. Ahmed *et al.*, “Significant Reduction in Thermal Conductivity and Improved Thermopower of Electron-Doped Ba_{1-x}La_xTiO₃ with Nanostructured Rectangular Pores,” *Adv. Electron. Mater.*, vol. 7, no. 4, pp. 1–10, 2021, doi: 10.1002/aelm.202001044.
- [11] Z. Yang, Y. Huang, B. Dong, H. L. Li, and S. Q. Shi, “Sol-gel template synthesis and characterization of LaCoO₃ nanowires,” *Appl. Phys. A Mater. Sci. Process.*, vol. 84, no. 1–2, pp. 117–122, 2006, doi: 10.1007/s00339-006-3591-3.
- [12] C. Eylem *et al.*, “Unusual metal-insulator transitions in the LaTi_{1-x}V_xO₃ perovskite phases,” *Chem. Mater.*, vol. 8, no. 2, pp. 418–427, 1996, doi: 10.1021/cm950351q.
- [13] N. Menyuk, K. Dwight, and P. M. Raccach, “Low temperature crystallographic and magnetic study of LaCoO₃,” *J. Phys. Chem. Solids*, vol. 28, no. 4, pp. 549–556, 1967, doi: 10.1016/0022-3697(67)90085-6.
- [14] G. Maris, Y. Ren, V. Volotchaev, C. Zobel, T. Lorenz, and T. T. M. Palstra, “Evidence for orbital ordering in LaCoO₃,” *Phys. Rev. B - Condens. Matter Mater. Phys.*, vol. 67, no. 22, pp. 1–5, 2003, doi: 10.1103/PhysRevB.67.224423.
- [15] V. Tuyikeze, L. H. Omari, and F. Fraija, “Isovalent Doping Effect on Structural, Optical Properties and Dispersion Parameters of Layered Perovskite La_{2-x}A_xTi₂O₇ (A = Bi, Ce, and Y, With x = 0.0 and 0.1),” vol. 7, 2021, [Online]. Available: <https://doi.org/10.21203/rs.3.rs-193967/v1>
- [16] P. G. Radaelli and S. W. Cheong, “Structural phenomena associated with the spin-state transition in (formula presented),” *Phys. Rev. B - Condens. Matter Mater. Phys.*, vol. 66, no. 9, pp. 1–9, 2002, doi: 10.1103/PhysRevB.66.094408.
- [17] H. W. Jang *et al.*, “Metallic and insulating oxide interfaces controlled by electronic correlations,” *Science (80-.)*, vol. 331, no. 6019, pp. 886–889, 2011, doi: 10.1126/science.1198781.
- [18] D. Grossin and J. G. Noudem, “Synthesis of fine La_{0.8}Sr_{0.2}MnO₃ powder by different ways,” *Solid State Sci.*, vol. 6, no. 9, pp. 939–944, 2004, doi: 10.1016/j.solidstatesciences.2004.06.003.
- [19] M. Tsubota *et al.*, “Hole-doping and pressure effects on the metal-insulator transition in single crystals of Y_{1-x}Ca_xTiO₃ (0.37 ≤ x ≤ 0.41),” *J. Phys. Soc. Japan*, vol. 72, no. 12, pp. 3182–3188, 2003, doi: 10.1143/JPSJ.72.3182.
- [20] V. A. Dudnikov, Y. S. Orlov, N. V. Kazak, M. S. Platonov, and S. G. Ovchinnikov, “Anomalies of the electronic structure and physical properties of rare-earth cobaltites near spin crossover,” *JETP Lett.*, vol. 104, no. 8, pp. 588–600, 2016, doi: 10.1134/S002136401620011X.
- [21] K. Kaminaga *et al.*, “A divalent rare earth oxide semiconductor: Yttrium monoxide,” *Appl. Phys. Lett.*, vol. 108, no. 12, pp. 1–5, 2016, doi: 10.1063/1.4944330.
- [22] G. Thornton, B. C. Tofield, and A. W. Hewat, “A Neutron Diffraction Study of LaCoO₃ in the Temperature Range 4.2 < T < 124 K,” *J. Solid State Chem.*, vol. 61, pp. 301–307, 1986.
- [23] Y. Zhao *et al.*, “Enhanced optical reflectivity and electrical properties in perovskite functional ceramics by inhibiting oxygen vacancy formation,” *Ceram. Int.*, vol. 47, no. 4, pp. 5549–5558, 2021, doi: 10.1016/j.ceramint.2020.10.139.